hcp Ising model in the cluster-variation approximation

R. McCormack, M. Asta, and D. de Fontaine
Department of Materials Science and Mineral Engineering, University of California, Berkeley, California 94720 and Materials Sciences Division, Lawrence Berkeley Laboratory, Berkeley, California 94720

G. Garbulsky and G. Ceder
Department of Materials Science, Massachusetts Institute of Technology, Cambridge, Massachusetts 02139
(Received 9 November 1992; revised manuscript received 26 April 1993)

We present a study of the hexagonal-close-packed Ising model for binary alloys within the cluster-variation approximation. Ground states of order stabilized by interactions that span the next-nearest-neighbor (NNN) distance (octahedron and all of its subclusters) were determined with the cluster-configuration polyhedron method. We predict 32 physically realizable ground states with stoichiometries A, AB, A_2B, A_3B, A_5B, and A_4B_3. Of these structures, six are stabilized by NN pairs and eight by NNN pairs; the remaining 18 structures require multiplet interactions for their stability. The results in this study are consistent with previous pair-interaction studies. Information concerning ground states and their domains of stability was then used in conjunction with the cluster-variation method (CVM) to calculate the finite-temperature phase equilibria for prototypical binary alloys. We present ordering phase diagrams computed with the CVM that contain all relevant ground states for both isotropic and anisotropic NN pair interactions. The results of the ground-state and CVM calculations are compared with those for ordering on the face-centered-cubic lattice.

I. INTRODUCTION

In many problems concerning phase equilibria of binary alloys A_xB_{1-x}, the thermodynamic behavior of (solid) alloys can be approximated by an Ising model. The configurational energy associated with a given arrangement of atoms is then calculated using the Ising-model Hamiltonian with a specified set of effective interaction parameters. These interactions can either be pairwise or multiatom, depending on the level of complexity required by the problem at hand. In general, the problems associated with the configurational statistical mechanics become more intractable as the range of the interaction increases. For either antiferromagnetic or ferromagnetic interactions on the chosen lattice, there are two distinct, yet related, domains of study: (a) analysis of the structures with the lowest *configurational* energy (ground states) as a function of composition at $T=0$ K and (2) analysis of finite-temperature phase behavior.

Several approximate methods of computing ground states of the Ising model on a given lattice have been used, most of which revolve around constructing a set of constraints on some set of configurational variables. The methods of Allen and Cahn[1] and Kanamori[2] have been widely used for ground states of binary alloys. The technique of sublattice division[3] can also be used to enumerate sets of possible structures, for which the energies can then be calculated and possible ground states determined. Ground-state analyses have been performed for numerous Ising lattices (see Ref. 4 for a complete listing), but in the field of alloy theory, perhaps the most widely studied of these are the fcc and bcc lattices, since ordered superstructures based on these parent lattices appear frequently in binary-alloy phase diagrams. Ordered superstructures of hcp (some of which are closely related to fcc superstructures) also appear in alloy systems such as Ti-Al and Cd-Mg. However, hcp ground states have not been analyzed as extensively as those of fcc and bcc.

The study of finite-temperature equilibrium can be carried out using any number of statistical-mechanical methods. The cluster-variation method[5] (CVM) is a generalized mean-field theory; the molecular-field or Bragg-Williams (BW) approach[6] and the Bethe approximation[7] are the point and pair approximations of the CVM, respectively. Additional (non-mean-field) theories for computing phase equilibria include Monte Carlo simulation,[8] renormalization-group theory,[9] and transfer-matrix techniques.[10] As a mean-field theory, the CVM yields classical critical exponents. However, by using higher-order approximations in the CVM entropy, extremely accurate transition temperatures can be determined. In particular, the CVM is a simple and very useful method for studying first-order transitions, and for this reason, it will be used in the present analysis. The CVM has been formulated in several ways, but the form that will be used here is based on the orthonormal cluster expansion of Sanchez, Ducastelle, and Gratias.[11] This formulation of the CVM involves an expansion of the energy in terms of multisite cluster functions; cluster probabilities used for computation of the entropy are also written as an expansion in these variables. The ground-state problem can also be formulated in this framework, where one uses the cluster expansion of the probabilities to obtain the necessary constraints in the analysis. We will hereafter refer to this ground-state method as the *cluster-configuration polyhedron* method (CCPM). The CCPM has been used for prototype studies on the bcc, fcc, and hcp lattices (see Ref. 4 for a summary).

An extensive study of hcp ground states which goes beyond pair interactions has not, to our knowledge, been

performed previously using the CCPM, although ground-state searches have been done using several other methods.[12–16] In this paper we consider the hcp analog of the fcc tetrahedron-octahedron (TO) approximation. The *complete* hcp ground-state search is performed in this approximation, for which interactions corresponding to clusters up to the octahedron are included. The uniqueness of the present study resides in the inclusion of multiatom interactions which, to our knowledge, no previous hcp ground-state searches have considered. Multiatom interactions have been shown to be important in several previous studies,[17–19] and they should be included in the ground-state search to obtain the most general results.

For a given Ising Hamiltonian, the CVM free energy can be computed for any of the hcp ground states found above. Once the free energy has been computed for all phases which are ground states for the given set of interactions, binary concentration-temperature (c-T) phase diagrams are synthesized using standard common-tangent constructions. In this paper we present several prototype-ordering phase diagrams with free energies computed for all relevant ground states. No previous CVM computations for hcp included all of the ground states for either isotropic or anisotropic pair interactions.[20–22]

The paper is organized as follows. A brief discussion of the formalism is presented in Sec. II. Results of the TO hcp ground-state analysis are given in Secs. III A and III B, and these results are discussed in Sec. III C, where a comparison is made with previous hcp studies and with analogous fcc results. Section IV is devoted to CVM prototype-ordering phase-diagram results and to a discussion of these results. One main objective of this paper is to point out the analogies and differences between the hcp and fcc Ising models for both ground states and finite-temperature behavior.

II. FORMALISM: CONFIGURATIONAL THERMODYNAMICS

Ising models are typically used to examine the decoration of a rigid lattice with various configurations of "atoms," and the Hamiltonian used defines the energy of these arrangements. In the case of a binary alloy with two atoms A and B, one assigns an atom to every site in the lattice (assuming that vacancies are not allowed). This assignment does not require atoms to lie directly on lattice sites. It is only necessary that the assignment be unambiguous; i.e., exactly one atom is associated with a given site.[23] One then specifies the pair and/or multiatom effective interactions between sites in the lattice, which defines the configurational energy of the system. Once the Ising model is formulated, any number of statistical-mechanical methods can be used to examine configurational energies, but in this paper we will be using the cluster-variation method.

A. Cluster-variation method

The cluster-variation method (CVM) was originally proposed by Kikuchi in 1951 (Ref. 5) to treat cooperative phenomena in solids. The basic goal of the CVM is to derive a hierarchy of approximations for the configurational entropy of the Ising lattice which converge to the exact solution of the Ising model. To this end one considers configurations of atoms on various clusters of atomic sites, with these clusters defined by the level of approximation used. The level of approximation of the hierarchy is specified by defining *maximal cluster(s)* of atomic sites. All possible combinations of subclusters up to and including this maximal cluster are treated as being correlated. A detailed discussion of the CVM and related topics can be found in a number of references.[4,5,23–29]

The essence of the CVM lies in minimizing a suitably constructed free energy with respect to a chosen set of configurational variables. A particularly convenient formulation for this set of variables is provided by the method of cluster expansion put forth by Sanchez, Ducastelle, and Gratias[11] to describe any function of configuration in multicomponent systems. The cluster expansion (see also Refs. 27–29) is based on an expansion in terms of an independent set of multisite *cluster functions;* it was originally proposed by Sanchez and de Fontaine[30] that this formulation be used to describe binary alloys. The cluster expansion for an arbitrary function of configuration in a binary system (the energy E, for example) on a given lattice is written as follows. Let the configuration of a lattice composed of N sites be written using the vector $\sigma=\{\sigma_1,\ldots,\sigma_N\}$, where the pseudospin variable $\sigma_{p_i}=-1$ $(+1)$ if an A (B) atom is associated with site p_i (in the case of a binary alloy). The configurational energy of the lattice can then be written as

$$E(\sigma)=\sum_{\alpha} V_{\alpha}\Phi_{\alpha}(\sigma)\ , \tag{1}$$

where α denotes a cluster of sites in the lattice, V_{α} is called the *effective cluster interaction* (ECI) for cluster α, and Φ_{α} is the *cluster function* for cluster α. If we write an abbreviated "site" vector for cluster α as $\alpha=\{p_1,\ldots,p_n\}$, where α consists of n lattice sites, then the cluster function Φ_{α} is defined as a product of the spins on the n sites:

$$\Phi_{\alpha}=\sigma_{p_1}\sigma_{p_2}\cdots\sigma_{p_n}\ . \tag{2}$$

These cluster functions form a complete orthonormal set defined with respect to an inner product which is a sum (trace) over all possible configurations σ.[11] The expectation values (ensemble averages) of the cluster functions are referred to as *correlation functions.*

The cluster expansion can be used to obtain the necessary information to compute the CVM free energy of a given structure. The internal energy is the expectation value of the configurational energy in Eq. (1). The general form of the configurational entropy in the CVM involves reduced-density matrices[11] (ρ_{α}^{J}), which we will hereafter refer to as *cluster probabilities;* ρ_{α}^{J} is defined as the ensemble probability of observing configuration J on cluster α. The internal energy and entropy can then be combined to express a general CVM free energy. Since group theory will be used to simplify the problem, the

free energy needs to be written using the symmetry of the structure under consideration (see Ref. 27):

$$f=\sum_{\Omega_S(\alpha)} V_\alpha m_\alpha \xi_\alpha + k_B T \sum_{\Omega_S(\beta)}^{\alpha_M} \gamma_\beta \sum_{J=1}^{n_\beta} \rho_\beta^J \ln \rho_\beta^J , \tag{3}$$

where f is the Helmholtz free energy per lattice point. The sum over $\Omega_S(\alpha)$ stands for a sum over crystallographic *orbits* of clusters up to the maximal cluster(s). The orbit of a cluster α in the structure S is defined as the set of all clusters of type α which are obtained by applying all space-group-symmetry operations of the structure S to the cluster. In other words, all clusters in the structure which are equivalent by symmetry are said to be in the same crystallographic orbit. In this way a single cluster in a given orbit is a representative of that orbit. The symmetry of the structure is implicit in the variable m_α, which is the number of α clusters per *atom* (multiplicity of α). The energy sum contains all clusters which are considered in the Hamiltonian, i.e., if one considers effective interactions up to and including only the nearest-neighbor pair, then the sum only contains terms for the empty (configuration independent), point, and nearest-neighbor pair clusters.

The second term in Eq. (3) is the expression for the negative of the CVM entropy (multiplied by absolute temperature). The sum over β in this expression contains all subclusters of the maximal CVM cluster(s) (α_M); it should be noted that the energy expansion must contain subclusters of the maximal cluster(s), but not necessarily *all* subclusters. The coefficient γ_β is the Kikuchi-Barker (KB) coefficient for cluster β. This is a strictly geometrical quantity and can be determined using a set of recursive relations originally derived by Barker[25] (see also Ref. 11). The essential approximation of the CVM is to factorize the density matrix over a restricted set of clusters, i.e., clusters up to and including the maximal cluster.[11,27] In order to minimize the free-energy functional, it is desirable to write the cluster probabilities in Eq. (3) as a cluster expansion, where the function of configuration is now the probability of observing a given configuration on a cluster of atomic sites. The coefficients of the cluster probability expansion form the elements of the so-called configuration matrix, the C matrix (see Refs. 27 and 30).

Once one has chosen a structure to be examined, the CVM problem reduces to finding a set of symmetry-related properties (subclusters of α_M, γ_β, m_α, C matrix) and the set of effective cluster interactions for the physical system under study (V_α). In principle, if one possesses all of this information, one can compute the equilibrium CVM free-energy and equilibrium values of the correlation functions by minimizing Eq. (3) with respect to the correlation functions. Effective cluster interactions for real systems (see Refs. 28 and 29) can be obtained through any number of techniques, for example, the method of direct configurational averaging (DCA),[31] the generalized perturbation method (GPM),[32] the embedded-cluster method (ECM),[33] and the Connolly-Williams (or inversion) method.[34] In this paper we are not concerned with the calculation of ECI's using any of these methods. Rather, we are interested in performing a general parametric study using different possible values of the interactions.

B. Ground-state analysis

The determination of the ordered structures which possess the lowest energy at $T=0$ K (ground states) is of great importance, since it is expected that these structures will also be observed at finite temperature, depending on the set of effective cluster interactions. As stated previously, several methods exist for finding ordered ground states (GS's) given a certain range of interaction. One such formulation (the CCPM) involves the use of "orbit- (or lattice-) averaged" cluster probabilities to obtain the set of constraints on allowable structures. The lattice-averaged cluster probabilities are then written as a linear combination of lattice-averaged cluster functions (using the C matrix for the disordered phase) which are defined as

$$\bar{\Phi}_\alpha = \frac{1}{N_\alpha} \sum_{\alpha_i \in \Omega_L(\alpha)} \Phi_{\alpha_i} , \tag{4}$$

where α_i denotes a cluster which is in the orbit $[\Omega_L(\alpha)]$ of cluster α *in the disordered phase* and N_α is the number of clusters in the orbit. This quantity $\bar{\Phi}_\alpha$ is simply the average of the cluster function Φ_α for all clusters α in the lattice.[27] In any realizable ground state, the CCPM requires that the probability of observing a given configuration on one of the chosen maximal clusters at $T=0$ K (the orbit average) is constrained to values greater than or equal to zero.[27] The goal of the ground-state analysis is then to minimize the configurational energy constructed[4,27] using Eq. (1). Thus we are minimizing a linear function subject to a set of linear constraints (a classical linear-programming problem).

At a given level of approximation, there will be q-independent cluster functions with r distinct orbit-averaged cluster probabilities. If each cluster probability is individually set equal to zero, the resulting equation defines a hyperplane in the multidimensional vector space spanned by the cluster functions (dimension q). It can be shown that the set of r hyperplanes can be used to obtain a convex polytope of dimension q which is called the *configuration polyhedron* (CP).[4] The set of allowed values of the cluster functions lie on or within this polyhedron, and thus one can obtain bounds for the energy. It is well known in such problems that the minimum values of the energy will be obtained when the cluster functions correspond to one of the vertices of the CP.[4] Any structure which has its cluster functions defined by a point on the line joining two vertices will be degenerate with respect to the appropriate linear combination of the vertices which define the edge and similarly for points on faces of the polytope. Thus the ground-state problem reduces to finding the vertices of the CP for the given set of cluster functions. The enumeration of all vertices of a polytope defined by its hyperplanes is a (linear-programming) problem which occurs frequently in operations research, and the same methods can be used in the current analysis. For an overview of the different algorithms

used for this problem, the interested reader is referred to Refs. 35–37.

The range of interaction treated in the ground-state search is determined by the clusters which are used to construct the constraints. In principle, one can construct the dual-space map corresponding to this CP (see, for example, Ref. 4), in which the vector space changes from configurational coordinates to interaction coordinates. This map illustrates which vertices are stable for various ranges of the interactions. It should be noted that not all of the ECI's contained in the given level of approximation act to stabilize a given structure. For example, some structures may be stabilized by only pair interactions; i.e., no multibody interactions are needed in the energy expansion to make the structure a ground state. In order to determine what set of interactions stabilize what structures, one can project the CP down to the space spanned by the cluster functions (interactions) of interest.[4]

One problem which is inherent in the method described above is that some vertices of the CP may correspond to structures which are not physically realizable; such vertices are called *inconstructible.* This type of vertex often occurs in ground-state searches for lattices which possess a high degree of frustration, i.e., the fcc and hcp lattices. In most cases one can prove that a vertex is inconstructible by utilization of the C matrix (see Sec. III C).

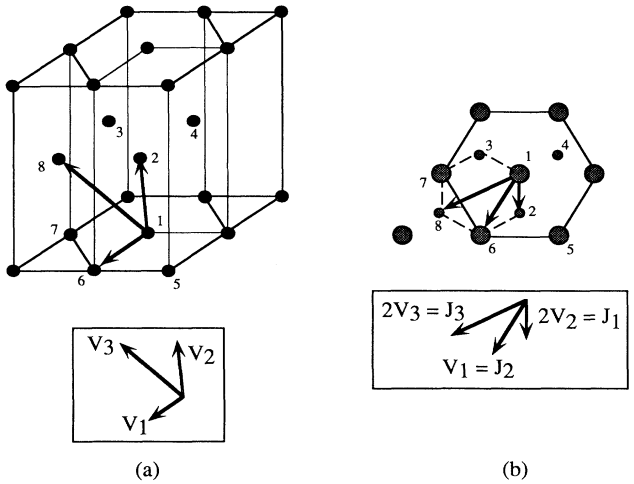

FIG. 1. (a) Three-dimensional hexagonal-close-packed structure. Effective pair interactions V_1, V_2, and V_3 correspond to sites (1,6), (1,2), and (1,8), respectively. (b) hcp structure in (001) projection, illustrating how the three-dimensional structure can be mapped onto a two-dimensional hexagonal lattice with interactions J_1–J_3.

III. hcp GROUND-STATE ANALYSIS

The hexagonal-close-packed (hcp) structure is shown in Figs. 1(a) and 1(b); Fig. 1(b) is the (001) projection of Fig. 1(a) and will be used extensively. The nearest-neighbor (NN) pairs indicated in Fig. 1(a) as V_1 and V_2 are crystallographically distinct, but when the hcp c/a is *ideal,* they span the same distance within the structure. The next-nearest-neighbor (NNN) pair is indicated as V_3 in Fig. 1(a). In the remainder of this study, when $V_1 = V_2$, we will say that the interactions are *isotropic;* if $V_1 \neq V_2$, the interactions will be referred to as *anisotropic. Even with an ideal c/a ratio,* the interactions V_1 and V_2 may be different because they are distinct by symmetry.

A. hcp cluster functions in the TO approximation

As stated in Sec. II B, in the CCP method, one needs to consider some set of clusters (also referred to as the *basis* clusters) in order to obtain the constraints used in the ground-state (GS) problem. The CCP analysis has been done for the fcc lattice using the tetrahedron (see Ref. 4) and tetrahedron-octahedron[17] approximations. The analogous computations in hcp correspond to the NN tetrahedron-triangle (TT) and the NNN tetrahedron-octahedron (TO) approximations of the hcp structure. In a calculation which accurately treats correlation within a given distance, it is then necessary to consider all symmetry-distinct clusters which span this distance. The analysis of all symmetry-distinct clusters up to NNN has already been performed for the hcp structure.[26] A correct hcp CVM entropy in the TO approximation must consider subclusters of both the NN tetrahedron (1,2,3,4) and the octahedron (1,2,3,6,7,8) [see Fig. 1(a)]. The cluster functions which correspond to the seven clusters (Φ_1, Φ_2, Φ_3, Φ_5, Φ_6, Φ_8, and Φ_9) in Table I form the basis set for the TT CVM approximation in hcp; the cluster functions for all 14 clusters in Table I form the basis for the TO approximation. The ground-state analysis will be performed in the 14-dimensional configuration space spanned by the TO cluster functions.

B. hcp tetrahedron-octahedron vertex enumeration

The independent variables which will be used in the GS analysis have now been listed. The constraints used in the TO ground-state analysis are formulated using the expansion coefficients of the cluster probabilities (i.e., the C matrix computed for the 14 cluster functions given in Table I). Cluster probabilities are considered for all symmetry-distinct configurations on the NN tetrahedron (Φ_9) and the octahedron (Φ_{14}). If constraints are satisfied for these basis clusters, then they are also satisfied for all of their subclusters.[11]

Computation of the C-matrix coefficients can be performed in several ways. Sanchez and de Fontaine[30] present a detailed example for several maximal clusters in the fcc lattice; the C matrices in these examples can be generated by hand. When one uses large maximal clusters such as the fcc 13+14 point approximation,[30] group-theoretical techniques are well suited (if not necessary) for computing the C matrix. Ceder[27] used group theory to generate the disordered fcc 13+14 C matrix (see also Ref. 19), and those techniques will be used in the present analysis.

Once the C matrix (or the relevant submatrix) has been computed for the *disordered* hcp structure,[27] the ground-state analysis can be performed. The configuration po-

TABLE I. Tetrahedron-octahedron CVM cluster analysis for the disordered hcp structure. Information by column is as follows: (1) independent cluster functions; (2) symbol for cluster function; (3) sites for cluster from Fig. 1(a); (4) multiplicity of cluster (clusters per atom), (5) γ_β coefficients (TT approximation), and (6) γ_β coefficients (TO approximation).

Cluster function	Symbol	Site(s)	Multiplicity (m_β)	γ_β (TT)	γ_β (TO)
Point	Φ_1	1	1	5	−1
IP pair	Φ_2	1,6	3	−3	3
OP pair	Φ_3	1,2	3	−3	3
NNN pair	Φ_4	3,6	3		0
Triangle (basis)	Φ_5	1,6,7	1	1	−1
Triangle (tet.)	Φ_6	2,3,4	1	−1	−1
3-pt	Φ_7	1,3,6	12		0
Triangle (OP)	Φ_8	1,2,6	6	0	−6
Tetrahedron	Φ_9	1,2,3,4	2	2	2
4-pt[1]	Φ_{10}	2,3,6,7	3		0
4-pt[2]	Φ_{11}	1,2,3,6	6		0
4-pt[3]	Φ_{12}	1,2,6,7	6		0
5-pt	Φ_{13}	1,2,3,6,7	6		0
Octahedron	Φ_{14}	1,2,3,6,7,8	1		1

lyhedron in the tetrahedron-octahedron approximation is the polytope formed by 21 hyperplanes (8 tetrahedron and 13 octahedron cluster probabilities in the C matrix) in the 14-dimensional space spanned by the cluster functions in Table I. The vertices of this polytope were enumerated using the algorithm proposed by Mattheiss.[38]

C. hcp TO ground states: Results and discussion

The full vertex search in the hcp TO approximation yielded a total of 172 vertices. All ground states with stoichiometries other than AB are symmetric with respect to the exchange of A and B atoms (i.e., there is a $1/-1$ degeneracy). The number of distinct vertices (degeneracy removed) is 111, 50 with stoichiometry AB and 61 non-AB vertices. The set of cluster functions which correspond to a particular vertex is not directly useful, and so one must construct the physical structure(s) which corresponds to the vertices (if such structures exist). Several approaches are viable when constructing the ground states, but the simplest involves using the previously derived C matrix to determine which of the configurations on the basis clusters will appear in the structure of a given vertex. The problem then reduces to tiling the hcp lattice with the configurations corresponding to the nonzero cluster probabilities such that (1) no inconsistencies are found and (2) the resulting structure has lattice-averaged cluster functions which correspond with the vertex in question. If no such tiling exists, then the vertex is inconstructible.

In many cases more than one structure can correspond to a given set of cluster functions. This is the case, for example, when structures can be related by antiphase boundaries (APB's), e.g., the $L1_2$ and $D0_{22}$ superstructures of the fcc lattice[4] (degenerate within the NN distance). The structures which have the same cluster functions are energetically degenerate from the standpoint of the *finite* cluster expansion [Eq. (6)]. If the range of the expansion is increased, i.e., a larger maximal cluster is chosen, then the degeneracy can be broken.

When the vertices from the GS search are analyzed using the method outlined above, we find that only 32 of the 111 distinct vertices (i.e., those with degeneracy removed) are constructible; the other 79 are inconstructi-

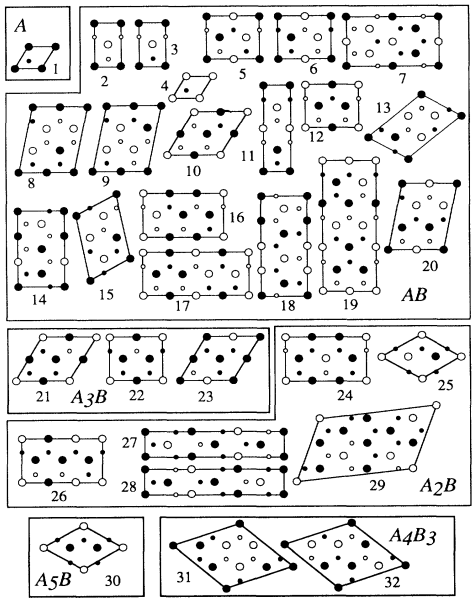

FIG. 2. Unit cells of the hcp tetrahedron-octahedron ground states in hcp (001) projection. Designations are consistent with those used in Table III. Structures of a given stoichiometry are grouped together in boxes for simplicity. It is clear that many of the structures predicted have unit cells larger than the range of interaction in the TO approximation. In addition, no structures are predicted with a periodicity which is greater than 1 along the z direction.

ble. The physically realizable ground states are given in Table II with the values of their lattice-averaged cluster functions (vertex coordinates). The realizable ground states predicted have stoichiometries A, AB, A_2B, A_4B_3, A_3B, and A_5B. A complete listing of the ground states is given in Table III with their stoichiometry, prototype (if applicable), Strukturbericht designation (if applicable), range of interactions required for stability (see below), and fcc structural analogs (if possible). It should be noted that fcc analogs are not necessarily stabilized by the same range of interactions. The most common experimentally observed hcp-based superstructures are those designated $B19$, $D0_{19}$, and $D0_a$. Hereafter, we will refer to all phases by their Strukturbericht designations (if possible) or by their stoichiometry followed by the number of the GS in Table III.

Unit cells which correspond to all ground states are given in Fig. 2 in [001] projection; these cells do not necessarily correspond to the unit cell which possesses the highest symmetry. The space-group symmetry of those structures with Strukturbericht designations or prototypes can be found in standard references;[39,40] the space groups for some of the other pair GS's can be found in Ref. 15. A knowledge of the space groups and Pearson symbols for all of the predicted ground states might allow the determination of more prototypes. The only complication in this approach is that one needs to include all symmetry-allowed relaxations when comparing with possible prototypes. It is interesting to note that several structures with large unit cells [e.g., $AB(17-19)$, $A_2B(29)$] are ground states despite the relatively limited range of interaction. The range of interaction is not actually correlated with the unit-cell size of ground states; this fact is intimately related to the conception of the ground states as a tiling of the lattice with the configurations which have nonzero cluster probabilities. Note also that we predict no ground states with a periodicity in the z direction larger than 1.

In the TO approximation, it is possible to have multibody interactions corresponding to any subclusters of the tetrahedron or octahedron which have more than two points. The question remains as to which of the vertices

TABLE II. Lattice-averaged cluster functions for hcp ground states in the tetrahedron-octahedron approximation. The clusters which correspond to each cluster function (Φ_α) are given in Table I.

No.	$\bar{\Phi}_1$	$\bar{\Phi}_2$	$\bar{\Phi}_3$	$\bar{\Phi}_4$	$\bar{\Phi}_5$	$\bar{\Phi}_6$	$\bar{\Phi}_7$	$\bar{\Phi}_8$	$\bar{\Phi}_9$	$\bar{\Phi}_{10}$	$\bar{\Phi}_{11}$	$\bar{\Phi}_{12}$	$\bar{\Phi}_{13}$	Φ_{14}
1	1	1	1	1	1	1	1	1	1	1	1	1	1	1
2	0	$-\frac{1}{3}$	$-\frac{1}{3}$	1	0	0	0	0	1	1	$-\frac{1}{3}$	$-\frac{1}{3}$	0	1
3	0	$-\frac{1}{3}$	$\frac{1}{3}$	-1	0	0	0	0	-1	1	$-\frac{1}{3}$	$\frac{1}{3}$	0	-1
4	0	1	-1	-1	0	0	0	0	-1	1	1	-1	0	-1
5	0	$-\frac{1}{3}$	$-\frac{1}{3}$	$\frac{1}{3}$	0	0	0	0	1	$-\frac{1}{3}$	$\frac{1}{3}$	$\frac{1}{3}$	0	-1
6	0	$-\frac{1}{3}$	$\frac{1}{3}$	$-\frac{1}{3}$	0	0	0	0	-1	$-\frac{1}{3}$	$\frac{1}{3}$	$-\frac{1}{3}$	0	1
7	0	0	0	$\frac{1}{3}$	0	0	0	0	-1	$-\frac{1}{3}$	0	0	0	-1
8	0	$-\frac{1}{9}$	$\frac{1}{3}$	$-\frac{1}{9}$	$-\frac{2}{3}$	$\frac{2}{3}$	$-\frac{2}{9}$	$\frac{2}{9}$	$-\frac{1}{3}$	$-\frac{1}{3}$	$\frac{1}{9}$	$-\frac{1}{3}$	$\frac{4}{9}$	$\frac{1}{3}$
9	0	$-\frac{1}{9}$	$\frac{1}{3}$	$-\frac{1}{9}$	$\frac{2}{3}$	$-\frac{2}{3}$	$\frac{2}{9}$	$-\frac{2}{9}$	$-\frac{1}{3}$	$-\frac{1}{3}$	$\frac{1}{9}$	$-\frac{1}{3}$	$-\frac{4}{9}$	$\frac{1}{3}$
10	0	0	0	-1	0	0	0	0	1	1	0	0	0	-1
11	0	$\frac{1}{3}$	$\frac{1}{3}$	$\frac{1}{3}$	0	0	0	0	1	$-\frac{1}{3}$	$-\frac{1}{3}$	$-\frac{1}{3}$	0	-1
12	0	0	0	$-\frac{2}{3}$	0	0	0	0	1	$\frac{1}{3}$	$-\frac{1}{3}$	$\frac{1}{3}$	0	0
13	0	$-\frac{1}{5}$	$\frac{1}{15}$	$\frac{1}{15}$	$-\frac{2}{5}$	$-\frac{2}{5}$	$-\frac{2}{15}$	$\frac{2}{15}$	$-\frac{3}{5}$	$-\frac{1}{3}$	$\frac{1}{5}$	$-\frac{1}{15}$	$\frac{4}{15}$	$-\frac{1}{5}$
14	0	$-\frac{1}{9}$	$-\frac{1}{9}$	$-\frac{1}{9}$	$-\frac{2}{3}$	$-\frac{2}{3}$	0	$\frac{2}{9}$	$-\frac{1}{3}$	$-\frac{1}{3}$	$\frac{1}{9}$	$\frac{1}{9}$	0	$\frac{1}{3}$
15	0	$-\frac{1}{5}$	$\frac{1}{15}$	$\frac{1}{15}$	$\frac{2}{5}$	$\frac{2}{5}$	$\frac{2}{15}$	$-\frac{2}{15}$	$-\frac{3}{5}$	$-\frac{1}{3}$	$\frac{1}{5}$	$-\frac{1}{15}$	$-\frac{4}{15}$	$-\frac{1}{5}$
16	0	$-\frac{1}{9}$	$-\frac{1}{9}$	$-\frac{1}{9}$	$\frac{2}{3}$	$\frac{2}{3}$	0	$-\frac{2}{9}$	$-\frac{1}{3}$	$-\frac{1}{3}$	$\frac{1}{9}$	$\frac{1}{9}$	0	$\frac{1}{3}$
17	0	$-\frac{1}{6}$	0	$-\frac{1}{3}$	$\frac{1}{2}$	$\frac{1}{2}$	$-\frac{1}{6}$	$\frac{1}{6}$	$\frac{1}{2}$	$\frac{2}{3}$	$-\frac{1}{3}$	$\frac{1}{6}$	0	0
18	0	$-\frac{1}{6}$	0	$-\frac{1}{3}$	$-\frac{1}{2}$	$-\frac{1}{2}$	$\frac{1}{6}$	$-\frac{1}{6}$	$\frac{1}{2}$	$\frac{2}{3}$	$-\frac{1}{3}$	$\frac{1}{6}$	0	0
19	0	$-\frac{1}{9}$	$\frac{1}{9}$	$-\frac{5}{9}$	$-\frac{2}{3}$	$\frac{2}{3}$	0	$\frac{2}{9}$	$\frac{1}{3}$	$\frac{1}{9}$	$-\frac{1}{9}$	$\frac{1}{9}$	0	$\frac{1}{3}$
20	0	$-\frac{1}{9}$	$\frac{1}{9}$	$-\frac{5}{9}$	$\frac{2}{3}$	$-\frac{2}{3}$	0	$-\frac{2}{9}$	$\frac{1}{3}$	$\frac{1}{9}$	$-\frac{1}{9}$	$\frac{1}{9}$	0	$\frac{1}{3}$
21	$\frac{1}{2}$	0	0	1	$-\frac{1}{2}$	$-\frac{1}{2}$	$\frac{1}{2}$	$-\frac{1}{2}$	-1	1	0	0	$\frac{1}{2}$	1
22	$\frac{1}{2}$	0	0	$\frac{2}{3}$	$-\frac{1}{2}$	$-\frac{1}{2}$	$\frac{1}{6}$	$-\frac{1}{2}$	-1	$\frac{1}{3}$	$-\frac{1}{3}$	$-\frac{1}{3}$	$-\frac{1}{6}$	0
23	$\frac{1}{2}$	0	$\frac{1}{3}$	0	$-\frac{1}{2}$	$-\frac{1}{2}$	$-\frac{1}{6}$	$\frac{1}{6}$	0	$-\frac{1}{3}$	0	$-\frac{1}{3}$	$-\frac{1}{6}$	0
24	$\frac{1}{3}$	$-\frac{1}{3}$	$\frac{1}{9}$	$\frac{1}{9}$	-1	-1	$-\frac{1}{9}$	$-\frac{1}{9}$	$-\frac{1}{3}$	$\frac{1}{9}$	$\frac{1}{9}$	$-\frac{1}{3}$	$\frac{1}{3}$	1
25	$\frac{1}{3}$	$\frac{1}{3}$	$-\frac{1}{3}$	$-\frac{1}{3}$	1	1	$-\frac{1}{3}$	$-\frac{1}{3}$	$\frac{1}{3}$	$-\frac{1}{3}$	$-\frac{1}{3}$	$\frac{1}{3}$	$\frac{1}{3}$	1
26	$\frac{1}{3}$	$-\frac{1}{9}$	$\frac{1}{9}$	$-\frac{1}{3}$	$-\frac{1}{3}$	$-\frac{1}{3}$	$-\frac{1}{3}$	$\frac{1}{9}$	$\frac{1}{3}$	$-\frac{1}{3}$	$\frac{1}{9}$	$-\frac{1}{9}$	$\frac{1}{3}$	1
27	$\frac{1}{3}$	$\frac{1}{9}$	$-\frac{1}{3}$	$\frac{1}{9}$	$\frac{1}{3}$	$\frac{1}{3}$	$-\frac{1}{9}$	$-\frac{5}{9}$	$-\frac{1}{3}$	$\frac{1}{9}$	$-\frac{1}{3}$	$\frac{1}{9}$	$\frac{1}{3}$	1
28	$\frac{1}{3}$	$\frac{1}{9}$	$\frac{1}{9}$	$\frac{5}{9}$	$\frac{1}{3}$	$\frac{1}{3}$	$-\frac{1}{9}$	$\frac{1}{3}$	1	$\frac{1}{9}$	$-\frac{1}{3}$	$-\frac{1}{3}$	$-\frac{5}{9}$	$-\frac{1}{3}$
29	$\frac{1}{3}$	0	$\frac{1}{3}$	$-\frac{1}{3}$	0	$-\frac{2}{3}$	0	0	0	$\frac{1}{3}$	$-\frac{1}{3}$	0	$-\frac{1}{3}$	-1
30	$\frac{2}{3}$	$\frac{1}{3}$	$\frac{1}{3}$	$\frac{1}{3}$	0	0	0	0	$-\frac{1}{3}$	$-\frac{1}{3}$	$-\frac{1}{3}$	$-\frac{1}{3}$	$-\frac{2}{3}$	-1
31	$\frac{1}{7}$	$-\frac{1}{7}$	$\frac{3}{7}$	$-\frac{1}{7}$	-1	$\frac{1}{7}$	$-\frac{3}{7}$	$\frac{1}{7}$	$-\frac{5}{7}$	$-\frac{1}{7}$	$\frac{3}{7}$	$-\frac{1}{7}$	$\frac{1}{7}$	1
32	$\frac{1}{7}$	$-\frac{1}{7}$	$-\frac{1}{7}$	$\frac{3}{7}$	$\frac{1}{7}$	-1	$\frac{1}{7}$	$\frac{1}{7}$	$-\frac{1}{7}$	$-\frac{1}{7}$	$\frac{3}{7}$	$\frac{3}{7}$	$\frac{1}{7}$	$-\frac{5}{7}$

TABLE III. Ground states in the hcp tetrahedron-octahedron approximation. A numerical designation is given in column 1, followed by the stoichiometry in column 2. If available, the prototype and Strukturbericht designation are given in columns 3 and 4, respectively. Column 5 indicates the range of interactions required for stability: I-NN pairs, II-NN and NNN pairs, III-multiplets which are subclusters of the TO, and IV-NN multiplets (subclusters in the TT approximation). The fcc analog is given in column 6, if such an analog exists.

No.	Concentration	Prototype	Designation	Range	fcc analog
1	A	Mg	$A3$	I	$A1$
2	AB	AuCd	$B19$	I	$L1_0$
3		CuTe		I	$AB(i)$[a]
4		WC	B_h	I	$L1_1$
5				II	40[b]
6				II	$AB(e)$[c]
7				III	$AB(b)$[c]
8				III	
9				III	
10				III	
11				III	$AB(a)$[c]
12–20				III	
21	A_3B	Ni_3Sn	$D0_{19}$	I	$L1_2$
22		β-Cu_3Ti	$D0_a$	II	$D0_{22}$
23				II	
24	A_2B			I	
25		B_2NdRh_3		II	
26				II	A_2B $C2/m$
27		Si_2Zr	$C49$	II	$MoPt_2$
28				III	$A_2B(c)$[c]
29				III	
30	A_5B	B_2NdRh_3		II	A_5B $C2/m$
31	A_4B_3			IV	
32				III	

[a]Designation of Ducastelle (Ref. 4).
[b]Designation of Kanamori and Kakehashi (Ref. 45).
[c]Designation of Sanchez and de Fontaine (Ref. 17).

in the ground-state analysis are stabilized by only effective pair interactions and which require multiatom interactions. One method of solving this problem is to project the configuration polyhedron from its 14-dimensional space down to a space spanned by various sets of clusters. In the present analysis, we can project onto spaces spanned by $\Phi_1-\Phi_3$ (for NN pair GS), $\Phi_1-\Phi_4$ (for NN+NNN GS), or to the space spanned in the TT analysis (multiplets within the NN; see Sec. III A). One then constructs a new polytope in the projection space which is the "convex hull" for the set of projected points. A summary of the results when these projections are performed is given in Table IV, where we indicate the number of distinct vertices, the number which are constructible, and the designations used in Table III.

Typically, one constructs so-called ground-state maps which show the stable phases as a function of the values of interactions. Such a map was constructed for NN pair interactions V_1 and V_2 where we computed the lowest-energy vertex as a function of interaction ratio (V_2/V_1) and normalized chemical field (μ/V_1). A map can be constructed for V_1 either positive or negative (corresponding to ordering and clustering, respectively). The ground-state map for $V_1<0$ only contains two ground

TABLE IV. Stable ground states for various sets of interactions. The configuration space indicates the set of clusters which span the space (see text). For approximations beyond NN pairs, there is overlap between the constructible ground states that each analysis predicts (indicated in parentheses; m designates a multiplet (GS). The designation in column 4 is the one used in Table III, given in the same order as the structures in parentheses in column 3.

Configuration space	Distinct vertices	Constructible	Designation
NN pairs	7	6	I
NN+NNN pairs	15	14(6+8)	I and II
TT	18	7(6+1m)	I and IV
TO	111	32(6+8+1m+17m)	I, II, IV, and III

states: $A3$ (disordered hcp, $\alpha = V_2/V_1 < \mu/6V_1$) and B_h ($\alpha > \mu/6V_1$). The ground-state map for $V_1 > 0$ is essentially identical to the map constructed by Bichara, Crusius, and Inden[41] for $V_3 = 0$; all GS's stabilized by interactions of type I (column 5, Table III) are present. The only discrepancy between the present analysis and that of Ref. 41 is that the present analysis predicts an inconstructible vertex (stoichiometry A_3B_2) in the region where Bichara, Crusius, and Inden[41] predict an infinite series of phases (discussed in Sec. III D 1). A map which includes V_1, V_2, and V_3 (restricting $V_1 = V_2$) is given in Ref. 12.

D. Discussion

1. *Comparison with previous hcp GS studies*

A comparison between the present results and those of Kudō and Katsura,[12] Singh and Lele,[13,14] and Singh, Singh, and Lele[15] is given in Table V. The results of the present study are shown in column 1, and those of the previous investigators are shown in the other columns using the notation adopted by these authors. All of the previous studies only considered pair interactions up to V_3 (either in two or three dimensions). All of the vertices present in our analysis which are stabilized by pair interactions appear in previous studies (omitting inconstructible vertices). Structures which are not obtained in the present analysis are as follows: A_9B_5, A_7B_5, A_2B^4, and A_2B^5. Singh and Lele[14] find all of these structures to be on edges or faces of their configuration polyhedron. The authors state that these structures are ground states, but in fact they are degenerate with respect to phase separation between the vertices which bound either the edge or plane. Hence they are absent from the present analysis and from that of Kudō and Katsura.[12] The studies of Refs. 12 and 14 predict several structures which are inconstructible (XIV and XV from Ref. 12); we have not included a comparison with these since it is not possible beyond the range of pair cluster functions and because the utility of comparing inconstructible GS's is limited. The 79 inconstructible GS's in the present analysis are not included in Table V.

Kanamori[16] performed a search on the plane hexagonal lattice in which he predicted an infinite series of ground states (devil's staircase) for interaction ratios greater than 1; he refers to these phases as the H_n, T_n, and R_n phases, formed by mixtures of different types of dislocation junctions in two dimensions (see Ducastelle[4] for a complete discussion). Some of the Kanamori designations correspond to phases in the present study: $AB(3) = R_1$, $DO_{19} = H_1$, and $B_h = T_\infty = R_\infty$. Bichara, Crusius, and Inden[41] mapped the two-dimensional results of Kanamori onto three dimensions [see Figs. 1(a) and 1(b)], constructing a series of ground-state maps for various values of the NNN pair interaction (V_3). As mentioned in the previous section, the map of Bichara, Crusius, and Inden[41] for $V_3 = 0$ predicts a devil's staircase of phases ($T_2 - T_\infty$ and $R_2 - R_\infty$) in the stability region of an A_3B_2 inconstructible vertex in our analysis. Kikuchi and Cahn[20] constructed a GS map for $\alpha > 0$ which is identical to the results we obtained; they also predicted an A_3B_2 inconstructible vertex, although it is impossible to know whether the vertex in this study is equivalent since they did not present any structural information.

The correspondence on the GS map between the inconstructible A_3B_2 vertex of the present work (and also Ref. 20) and the infinite series of ground states is by no means coincidential. The existence of a devil's staircase in hcp implies the following: An hcp ground-state analysis using *any* configurational polyhedron (CP) method *must* have at least one inconstructible vertex at any level of approximation which includes at least the NN pairs. This is most easily proven by contradiction: Assume a CP analysis produces a finite number of vertices, all of which are constructible. This implies that *at the level of approximation used* the analysis is *exact;* there are no more ground states for that set of interactions. This contradicts the existence of the devil's staircase predicted by Kanamori, and hence there must be at least one incon-

TABLE V. Comparison of present ground-state analysis with the studies of Refs. 12–15. Column 1 gives the number of the ground states (corresponding to Table VI). A blank entry indicates that a given ground state was not predicted. Ground states which are inconstructible are denoted (†), while those which are actually degenerate are indicated with (††). If a column is empty, this indicates that a comparison was not possible. The agreement is essentially quantitative for all pair ground states, but the previous studies were unable to predict all multiplet ground states (indicated with italics in column 1). Inconstructible GS's from the present analysis have not been included in column 1 for brevity.

No.	Isotropic hcp[a]	Plane hex.[a]	Configuration polyhedron[b]	Cluster method[c]	Sublattice method[d]
1	I	I	A	A	A
2	IX-1	V	AB^2	AB^2	AB^2
3	VII-2	III	AB^3	AB^3	AB^3
4	VII-1	II	AB^1	AB^1	AB^1
5	V	XIII	AB^4	AB^4	AB^4
6		XII	AB^5		AB^5
7–20					
21	VIII	IV	A_3B^1	A_3B^1	A_3B^1
22	III	IX	A_3B^3	A_3B^3	A_3B^3
23		XI	A_3B^2	A_3B^2	A_3B^2
24	IV-1	VI	A_2B^2		A_2B^2
25	VI-1	VIII	A_2B^1	A_2B^1	A_2B^1
26	VI-2				
27	IV-4	X	A_2B^3(II)		A_2B^3(II)
28,29					
30	II-2	VII	A_5B(I–III)	A_5B	A_5B
31,32					
			A_9B_5††		A_9B_5††
			A_7B_5††		A_7B_5††
			A_2B^4††		A_2B^4††
			A_2B^5††		
		XIV†	$A_2B(V)$†		
		XV†	$A_3B_2(V)$†		

[a]Reference 12.
[b]Reference 13.
[c]Reference 15.
[d]Reference 14.

structible vertex. In essence, this one inconstructible vertex allows for more and more of the devil's staircase to be predicted as the level of approximation in the GS analysis is increased (i.e., as the constraints are based on clusters which span a larger range).

The present analysis predicts 18 ground states which are stabilized by multiplet interactions (14 AB, 2 A_2B, and 2 A_4B_3). These structures are completely absent from all other studies[12–16,20] since previous authors only included pair interactions in their analyses. The omission of many-body interactions is unjustifiable on intuitive grounds, and it has also been demonstrated that such interactions are actually needed in order to explain the observed structures in numerous transition-metal-alloy systems[19,42] and also in the Ti-Al system.[43]

2. *Ground states on the hcp and fcc lattices*

One expects a one-to-one mapping of the fcc ground state onto hcp ground states (but *not* the converse) when only interactions between two close-packed planes are considered.[4] In particular, this will be true when considering NN and NNN pair interactions in hcp [sites $(1,2)\equiv(1,6)$ and (1,8), respectively, in Fig. 1(a)]. The analogy between fcc and hcp is clear when one constructs [111] projections of *two* close-packed planes for the fcc lattice; such a [111] fcc projection is identical to the [001] hcp projection. In order for there to be analogies between fcc and hcp, one must map the interactions in fcc onto the corresponding clusters in hcp. For example, consider fcc ground states in the tetrahedron approximation with NN pair ($V_{\rm NN}$) and NN triangle ($V_{\rm TR}$) interactions. hcp ground-state analogs will exist provided the hcp TT interactions obey the following (see Table I and Fig. 1): $V_{\Phi_2}=V_{\Phi_3}=V_{\rm NN}$ and $V_{\Phi_5}=V_{\Phi_6}=V_{\Phi_8}=V_{\rm TR}$. This mapping reestablishes the symmetries that are broken in passing from the fcc to the hcp lattice. The fcc-hcp ground-state analogy can be seen quite easily when one compares the NNN pair ground-state map for fcc (Refs. 4 and 44) and the NNN pair map for hcp (Ref. 12) with $V_1=V_2$: Their topologies are identical.

The analogs relevant to the current analysis are listed in Table III. The most commonly observed hcp structures ($B19$, $D0_{19}$, and $D0_a$) correspond to the fcc $L1_0$, $L1_2$, and $D0_{22}$ structures, respectively. If the ground-state search is performed in the tetrahedron approximation on the fcc lattice, the only ground states predicted are pure A, $L1_0$, and $L1_2$.[4] The fcc search in the TO approximation[17] yields six NNN pair GS's [$L1_1$, $D0_{22}$, $MoPt_2$, A_2B_2 ("40" in Ref. 45), A_5B, and A_2B] plus seven multiplet ground states [$AB(a,b,d,e,f)$, $A_2B(c)$, and $A_5B_3(g)$]. In the hcp TT approximation (equivalent to fcc tetrahedron), there are seven ground states (including one multiplet), as opposed to three in fcc with no multiplet GS. The hcp search in TO stabilizes the analogs of the fcc NNN pair GS's [B_h, $D0_a$, Si_2Zr, $AB(5)$, A_5B, and $A_2B(26)$] with the NNN pair acting to break the same NN pair degeneracies in hcp (e.g., between $D0_{19}$ and $D0_a$) that occur in fcc (between $L1_2$ and $D0_{22}$). As far as the multiplets are concerned, there are only hcp analogs for *four* of the fcc multiplet GS's: $AB(6,7,11)$ and $A_2B(28)$. The hcp analogs of the other three fcc multiplets [$AB(d,f)$ and $A_5B_3(g)$] lie on one-dimensional (1D) edges of the configuration polyhedron and hence are degenerate with respect to phase separation between the vertices that define the edge. All of the hcp GS's in Table III which do not have fcc analogs are probably stable over ranges of the interactions where the aforementioned mapping between fcc and hcp interactions is violated. It should also be mentioned that the interactions required to stabilize the analogous fcc and hcp ground states are not necessarily the same; for example, the hcp analog of $AB(e)$ from Ref. 17 (a multiplet ground state) is a NNN pair GS in hcp.

From the above discussion, the similarities between fcc and hcp are quite striking when considering only the *pair* ground states; in fact, the mapping is perfect since hcp analogs exist for all nine *pair* fcc GS's out to the NNN. However, there is a distinct departure between fcc and hcp when looking at all possible ground states. In the hcp TO, there are a total of 32 GS's, while there are only 16 in fcc; in other words, the differences in symmetry between fcc and hcp result in *twice* as many hcp ground states at the level of the TO. Although fcc and hcp are identical within two-close-packed planes when the hcp c/a ratio is ideal, they are not identical at the third plane. The existence of this third plane alters the symmetry such that even when the c/a ratio of hcp is ideal, it is possible for the values of interactions V_1 and V_2 to be different. In fcc, however, the NN pairs which correspond to V_1 and V_2 in hcp are identical by symmetry and must *always* have the same effective pair interaction. The relationship between the hcp c/a ratio and the values of V_1 and V_2 seems to be a point of confusion in numerous previous studies.[13–15,41] Previous authors tend to make the (incorrect) assertion that when the two NN pair interactions are different in hcp, this implies that the c/a ratio is nonideal.

IV. hcp CVM PHASE DIAGRAMS

In order to perform prototype CVM computations in either the TT or TO approximations of hcp, one needs (for all phases in the computation) the KB coefficients and multiplicities for each approximation (those for the disordered phase are in Table I) and also the C matrices. The entropy expressions and independent cluster functions (at the chosen level of approximation) must be derived for *each* phase which is a ground state for the set of interactions which are used. If a calculation is done using isotropic NN pairs in the TT entropy approximation, one would need to consider the disordered, $B19$, and $D0_{19}$ phases.[41]

The phase-diagram calculations in the following section necessitated computing the free energy for the $B19$, $D0_{19}$, and $A_2B(24)$ phases. Hence the independent cluster functions and entropy expressions were derived for all of these structures in both the TT and TO approximations. The results of the cluster determination are given in Table VI; it is clear that for the ordered phases, a complete presentation of the entropy expressions and cluster information would be quite lengthy. Hence that informa-

TABLE VI. Maximal (basis) clusters and number of independent cluster functions in the TT and TO approximations for the $A3$, $B19$, $D0_{19}$, and $A_2B(24)$ phases (Tr=triangles, T=tetrahedra, O=octahedra).

Structure	Basis clusters (TT)	TT cluster functions	Basis clusters (TO)	TO cluster functions
Disordered ($A3$)	1 Tr, 1 T	7	1 T, 1 O	14
$B19$	2 Tr, 2 T	19	2 T, 2 O	47
$D0_{19}$	2 Tr, 2 T	16	2 T, 2 O	37
$A_2B(24)$	2 Tr, 2 T	22	2 T, 2 O	57

tion will not be presented for all structures in all approximations. The increase in the number of independent cluster functions as a function of the symmetry of the phase is exhibited in Table VI.

A. Phase-diagram calculations

This section is devoted to a discussion of phase-diagram calculations using the CVM in combination with the ground-state results discussed in Sec. III. We will be considering *prototypical* ordering systems ($V_1>0$) for different values of V_2/V_1. Ordering will be considered for both isotropic and anisotropic NN pair interactions only; no multiplet interactions will be considered.

1. Isotropic interactions

Three ground states exist at the interaction ratio $V_2/V_1=1$: $B19$, $D0_{19}$, and $A3$. The A_3B_2 and $A_2B(24)$ phases share a single degenerate point in the GS map with the $B19$ and $D0_{19}$ phases when $V_2/V_1=1$, but these phases will not be considered. This is in fact an assumption, since it may be possible for the entropy to stabilize the degenerate phase(s) when $T>0$ K. A low-temperature expansion might be used to prove whether one of the degenerate phases would exist at finite temperature.[10]

CVM calculations were performed in the TT and TO approximations for $V_2/V_1=1$ for the three phases in question. The results of the phase diagram calculations are shown in Fig. 3 (bold lines=TT, thin lines=TO); since no odd-body interactions are considered, the phase diagram is symmetric around $c=0.5$, and hence only half of it is shown. The results of the Monte Carlo calculations of Crusius and Inden[46] (see Sec. IV C) are given with dashed lines. Both the $B19$ and $D0_{19}$ phases are seen to have a large stability range, and both congruently disorder at or near their respective stoichiometries. In addition, there is a eutectoid reaction in which the disordered phase decomposes into the $B19$ and $D0_{19}$ phases. This phase diagram is completely analogous to the prototype fcc phase diagram,[47] as will be discussed in Sec. IV C. Three things change when the level of approximation is increased from TT to TO: (1) Both the $D0_{19}$ and $B19$ order-disorder transition temperatures decrease, (2) the width of the two-phase regions decreases, and (3) the temperature at which the eutectoid reaction occurs decreases relative to the $B19$ and $D0_{19}$ transition temperatures.

2. Anisotropic interactions

Now we consider the range of interaction ratios $0<\alpha=V_2/V_1<1$. Four ground states exist for this set of interactions:[41] $B19$, $D0_{19}$, $A3$, and $A_2B(24)$. Calculations were performed for several values of α between zero and one; the phase diagrams for $\alpha=0.8$ and 0.5 (TT) are shown in Figs. 4 and 5, while that for $\alpha=0$ (TT and TO) is shown in Fig. 6. Monte Carlo results of Crusius and Inden[41] are superimposed on Figs. 4 and 6 (dotted lines) for comparison. When $\alpha=0.8$ (Fig. 4), the $A_2B(24)$ phase exhibits a very narrow range of stability and has a transition temperature which is much less than those of the $B19$ and $D0_{19}$ phases. The $B19$ and $D0_{19}$ transition temperatures have also decreased compared to the case of isotropic interactions. In the case where $\alpha=0.5$ (Fig. 5), it is seen that the $B19$, $D0_{19}$, and $A_2B(24)$ phases all have roughly the same relative stability, i.e., their transition temperatures are roughly the same. The $B19$ and $D0_{19}$ transition temperatures have again decreased compared to $\alpha=0.8$, and the $A_2B(24)$ transition temperature has increased by a comparable amount. When the in-

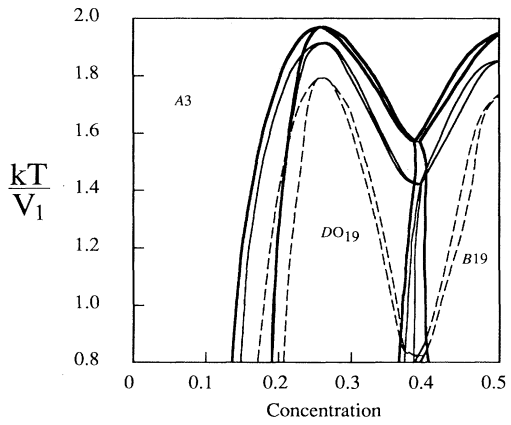

FIG. 3. hcp ordering phase diagram with isotropic NN pair interactions ($V_1=V_2>0$) computed in the CVM TT (bold lines) and TO (thin lines) approximations. The Monte Carlo results of Crusius and Inden[46] (Ref. 46) are superimposed (dashed lines). As the level of the CVM approximation is increased, the transition temperatures for the $B19$ and $D0_{19}$ phases decrease, as does the eutectoid temperature.

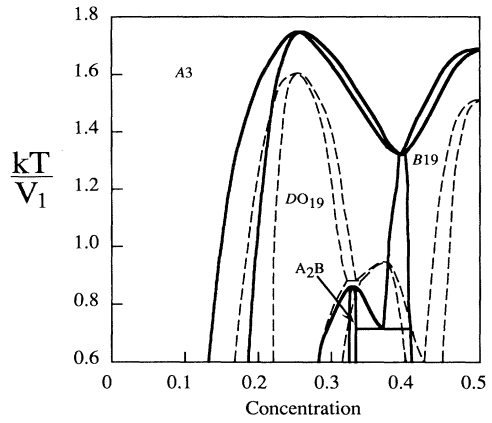

FIG. 4. hcp phase diagram for anisotropic interactions ($V_2=0.8V_1>0$) computed in the TT approximation (bold lines). The $A_2B(24)$ phase (now a ground state with this set of interactions) is only marginally stable and thus transforms into the $D0_{19}$ phase at a relatively low temperature. The Monte Carlo results of Crusius and Inden (Ref. 46) are superimposed (dashed lines). The Monte Carlo phase diagram has a different topology: The $A_2B(24)$ phase (significantly off stoichiometric) disorders into the hcp solid solution with two sets of eutectoid reactions occurring.

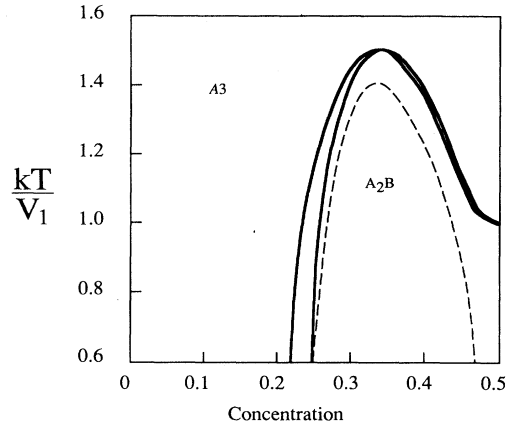

FIG. 6. hcp phase diagram for $V_2=0$, $V_1>0$. The $A_2B(24)$ phase is the only ordered ground state at this interaction ratio. All transitions are first order, except at $c=0.5$, where the transition is second order. The Monte Carlo results of Crusius and Inden (Ref. 46) are superimposed (dotted line); all of their transitions are second order, and no finite transition temperature exists at $c=0.5$ [see Wannier (Ref. 51)]. The CVM results are incorrect regarding the finite transition temperature at $c=0.5$ and the order of the transitions.

teraction ratio is zero, there is no coupling between the close-packed planes, and the $B19$ and $D0_{19}$ phases are no longer observed, as seen in Fig. 6. The TT and TO results for this calculation are identical, contrary to the trends (Sec. IV A 1) seen in the case for isotropic interactions (Fig. 3). When $\alpha=0$ the planes are decoupled, and the system is essentially two dimensional; the ordering within a single plane of the $A_2B(24)$ phase is identical to the ordering in the plane above or below it. The absence of the $B19$ and $D0_{19}$ phases when $\alpha=0$ is consistent with the GS map:[41] When $\alpha=0$ these two phases only exist at degenerate points.

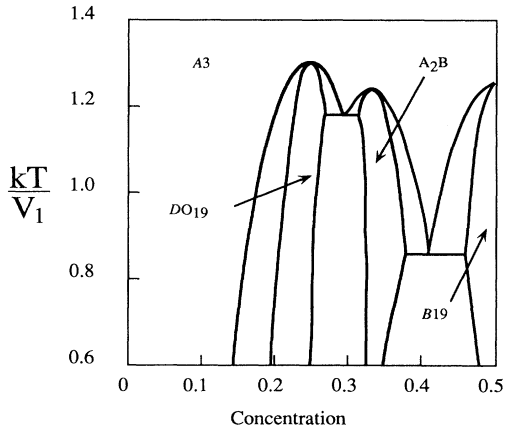

FIG. 5. hcp phase diagram for anisotropic interactions $V_2=0.5V_1>0$ (TT approximation only). At this interaction ratio, the $A_2B(24)$, $D0_{19}$, and $B19$ phases all have the same relative stability. The $A_2B(24)$ phase now disorders into the hcp solid solution, as opposed to the behavior observed for $\alpha=0.8$ (Fig. 5).

B. Discussion

1. *Comparison with previous prototype hcp phase diagrams*

The amount of work done on hcp phase diagrams is even more sparse than it is for hcp ground states. In two similar studies,[20,21] Kikuchi used the CVM in the TT approximation to determine the $A3$-$D0_{19}$ phase boundaries and the $A_2B(24)$ phase boundaries for $\alpha=0$; his studies do not consider equilibria between the $D0_{19}$ and $B19/A_2B(24)$ phases. Monte Carlo (MC) simulation on the hcp Ising lattice has been performed by Crusius and Inden[46] for $\alpha=1$ (Fig. 3), 0.8 (Fig. 4), and 0 (Fig. 6), and by Bichara, Crusius, and Inden[48] for $\alpha=1.5$ and 2.0. Studies using Monte Carlo simulation[49] and analytical techniques[50,51] have also been performed in the case when $\alpha=0$.

In the case of isotropic interactions, the hcp CVM and Monte Carlo phase diagrams are given in Fig. 3. As the level of the CVM approximation is increased from TT to TO, there is better agreement with the Monte Carlo results of Crusius and Inden.[46] In general, all of the transition temperatures (hcp$\rightarrow B19$, hcp$\rightarrow D0_{19}$, and hcp$\rightarrow D0_{19}+B19$) are lower in the Monte Carlo analysis. The TO results agree fairly well near the $B19$ and $D0_{19}$ transitions, but there is still quite a large discrepancy at the triple point. The same type of behavior is observed in CVM and MC calculations on the fcc lattice.[52] Finel[53] has actually shown, however, that by using a higher approximation in the CVM, it is possible to obtain virtually exact agreement between the MC method and the CVM.

When the interactions are anisotropic, the $A_2B(24)$ phase appears between the $D0_{19}$ and $B19$ phases in the phase diagram, and the hcp$\rightarrow A_2B(24)$ transition temperature depends on the value of the interaction ratio. The same behavior is observed in the MC analysis of Ref. 46, although the MC transition temperatures are again lower. The difference in transition temperatures makes a comparison between the Monte Carlo and CVM analyses difficult because the topologies of the phase diagrams are not the same. For example, in the case when $\alpha=0.8$ (Fig. 4), the CVM predicts $A_2B(24)$ to transform into the $D0_{19}$ phase ($c=0.33$, $kT/V_1=0.9$) with a eutectoid reaction still occurring between hcp, $B19$, and $D0_{19}$ ($c=0.4$, $kT/V_1=1.3$). The Monte Carlo study predicts the $A_2B(24)$ to disorder into the hcp solid solution, with two eutectoid reactions hcp$\rightarrow A_2B(24)+B19$ ($c=0.42$, $kT/V_1=0.6$) and hcp$\rightarrow A_2B(24)+D0_{19}$ ($c=0.33$, $kT/V_1=0.9$). If the level of the CVM entropy approximation were increased (i.e., to TO), then we would expect the hcp$\rightarrow B19+D0_{19}$ and $D0_{19}\rightarrow A_2B(24)$ transition temperatures to drop, with the former changing more than the latter. As the level of CVM approximation is successively increased (for $\alpha=0.8$), the transitions would most likely change to the point that the hcp$\rightarrow A_2B(24)+D0_{19}$, $A_2B(24)+B19$ reactions would be observed, in agreement with the Monte Carlo results. Indeed, the topologies of the CVM analysis for $\alpha=0.5$ (Fig. 5) and the MC phase diagram for $\alpha=0.8$ (dotted lines, Fig. 4) are quite similar, although the transition temperatures are different.

For $\alpha=0$ the only stable ordered phase is $A_2B(24)$ (Fig. 6); the largest disparity between the present results and those of the other previous studies occurs in this phase diagram. The CVM predicts a finite order-disorder transition temperature at $c=0.5$ and first-order transitions all the way across the concentration range except at the transition temperature for $c=0.5$, where the transition is second order. There is excellent agreement between the phase diagram of Fig. 6 and the CVM phase diagram of the 2D triangular lattice calculated by Burley.[22] The hcp Monte Carlo results of Crusius and Inden[46] predict a lower hcp$\rightarrow A_2B(24)$ transition temperature (as expected), and they predict only second-order transitions (dashed line, Fig. 6). Metcalf[49] performed Monte Carlo simulations on the two-dimensional triangular antiferromagnet (equivalent to ordering interactions with $\alpha=0$), finding results quite similar to those of Crusius and Inden. Houttapel[50] and Wannier[51] proved analytically that there is no long-range order (LRO) at $T=0$ K and $c=0.5$ for the 2D triangular antiferromagnet. Thus the analytical results[50,51] prove that the CVM result presented in Fig. 6 is incorrect regarding the finite transition temperature at $c=0.5$, and the Monte Carlo results[46] imply that the CVM is incorrect regarding the order of the transitions between hcp and $A_2B(24)$. This is perhaps not surprising since $A_2B(24)$ is essentially two dimensional, and it is known that mean-field models are less accurate as the dimensionality of the system decreases. The two-dimensional character of this phase is further illustrated by the equality of the TT and TO results for $\alpha=0$. The Hamiltonian for $\alpha=0$ only considers interactions within a plane. Hence the partition function for the entire system can be factored,[54] thus allowing the free energy to be written as a sum of free energies associated with the planes. Since the TT and TO approximations both span the NN distance *within* a plane, their results will be identical.

The differences between the CVM results and those obtained with Monte Carlo or other analytical techniques are due to the mean-field nature of the CVM, which neglects correlations beyond the maximal cluster. Hence, by increasing the size of the maximal cluster, the CVM takes longer-range correlations into account so that one expects the CVM results to converge to those of non-mean-field theories, consistent with present results and with previous studies in fcc (Refs. 52 and 53) (see Fig. 3).

2. *Ordering phase diagrams in fcc and hcp*

The analogies between fcc and hcp ground states were analyzed in Sec. III C 2, where the two NN pair interactions in hcp were assumed to be equal. It has been suggested[21] that the fcc and hcp phase diagrams for NN isotropic interactions should be identical. The hcp TT phase diagram with isotropic NN pair interactions (Fig. 4) shows a topology identical with the tetrahedron fcc phase diagram computed by Van Baal.[47] In the fcc case, it is also found that the ordering transition temperatures decrease as the level of the CVM entropy approximation is increased,[52,55] and the same is observed in hcp (Sec. IV A 1).

We performed calculations at high temperatures (i.e., above the order-disorder transition) for both fcc (T and TO) and isotropic hcp (TT and TO). We find the free energies of the disordered fcc and hcp phases consistently converge to slightly different results. This difference will of course lead to small but detectable differences in the fcc and hcp transition temperatures. It could be argued that computational inaccuracy is the cause for the discrepancies, but this is not the case. The systematic difference in transition temperatures has also been confirmed *analytically* by high-temperature expansion of the CVM free energy.[56]

It is possible to obtain fcc and isotropic hcp CVM free energies which are identical, but this involves imposing a constraint on the values that the hcp correlation functions may take. If we require all hcp correlations to be equal which were in the same orbit in fcc (e.g., the in-plane and out-of-plane NN pairs), then the fcc and hcp C matrices would be identical, and the CVM problems would be indistinguishable. This is an artificial situation, however, and we believe it is more correct to say the following: *At finite temperature, CVM computations of ordering on the fcc and isotropic hcp lattices are almost but not exactly equivalent, even with only interactions between two close-packed planes.* Despite the equivalence of the hcp and fcc Ising Hamiltonians when considering two close-packed planes, it is likely that the hcp phases can attain a higher entropy, and thus a lower free energy, by allowing certain correlations (which were equivalent in corresponding fcc phases) to take on different values.

All of the foregoing discussion has been for the case of isotropic pair interactions in hcp. If one allows for anisotropic pair interactions, then the equivalence between fcc and hcp CVM phase diagrams disappears. The simplest example of this is the TT phase diagram computed for $\alpha=0.5$, shown in Fig. 6. There is no fcc tetrahedron ground state which corresponds to $A_2B(24)$, and hence it would be impossible to obtain a tetrahedron fcc phase diagram with a topology like that in Fig. 6. In general, the symmetry of the hcp lattice allows for ground states which could never be observed on the fcc lattice, and hence the finite-temperature behavior would be different also.

V. CONCLUSION

Ising models are a powerful tool which can be used to study ordering phenomena for substitutional alloys on various lattices. Numerous studies in the past have considered ground states of order and finite-temperature behavior on the fcc and bcc lattices, but not nearly as much attention has been given to ordering in hexagonal-close-packed (hcp) alloys. Previous ground-state analyses in hcp have not allowed for the possibility of many-body interactions between atoms; these types of interactions are now known to play a potentially significant role in alloy phase stability.[17–19] The cluster-variation method (CVM) is well suited to treating interactions between clusters of atoms, but no ground-state searches have been done using the cluster-configuration polyhedron method, and few phase-diagram computations have been performed on hcp alloys using the CVM.

Thus we have presented a study of the hcp Ising model in the cluster-variation approximation. Ground states of order stabilized by interactions within the range of the octahedron were computed using the cluster-configuration polyhedron method. This ground-state method enumerates constraints on allowed structures by using the linear relationship between the probability of observing a given configuration on a cluster of atomic sites and an independent set of multisite configurational variables. In order to obtain all of the necessary constraints in the present analysis, all 14 symmetry-distinct subclusters of the octahedron and NN tetrahedron are required. The ground-state search yields results consistent with previous NN pair ground-state analyses, although we predict 18 new structures which are stabilized by multiplet interactions. In addition, it has been shown that any hcp ground-state search which uses a configuration polyhedron method must have at least one inconstructible vertex in order to be consistent with the infinite series of ground states predicted by Kanamori.[16]

Prototypical ordering phase diagrams for binary hcp alloys were computed for several different values of the two NN pair interactions using the CVM in the tetrahedron-triangle (TT) and/or tetrahedron-octahedron (TO) approximations. The analysis presented in this study considered equilibria between *all* ground states for the chosen interactions, which does not appear to have been done previously with the CVM. The observed phase equilibria for isotropic pair interactions are roughly analogous to ordering in fcc, but anisotropic pair interactions yield much more interesting behavior. Results are in generally good agreement with previous Monte Carlo studies of ordering in hcp alloys,[46] although discrepancies do exist due to the mean-field nature of the CVM. The CVM does, however, fail to correctly predict the behavior of ordering when the two close-packed planes in hcp are energetically decoupled: The order of the transitions is wrong, and the CVM incorrectly predicts a long-range-ordered phase at finite temperature for $c=0.5$.

Ordering in fcc and hcp is found to be similar, as one would expect. There are hcp analogs for all NN and NNN pair fcc ground states, but there are large discrepancies when considering the multiplet ground states. If the hcp NN pair interactions are restricted to being isotropic, it is expected that hcp and fcc ordering phase diagrams will be exactly the same. We do not find this to be the case: Small but consistent differences exist between the fcc and hcp results. The difference between fcc and hcp lies in the symmetry which each structure possesses. The fcc lattice and hcp structure are equivalent within two close-packed planes, but the existence of a third different plane makes the global symmetry different for each. Hence clusters of sites (and their corresponding interactions) which were equivalent by symmetry in fcc are no longer equivalent in hcp. As a consequence of this, the configurational entropy in hcp alloys can be distinct from that in fcc alloys even when the Hamiltonians are the same. Anisotropic interactions in hcp allow for new ground states to be stabilized which would not be observed in fcc, thus providing a much richer spectrum of possible finite-temperature behavior. Therefore to make generalizations about ordering in hcp based on fcc behavior is not strictly valid.

ACKNOWLEDGMENTS

The authors would like to acknowledge Chris Wolverton for numerous useful and stimulating discussions about the topics presented here. This work was supported by the Director, Office of Basic Energy Sciences, Materials Science Division of the U.S. Department of Energy under Contract No. DE-AC03-76SF00098 and also by the Department of the Army under Contract No. DAAL03-91-G-0268.

[1] S. M. Allen and J. W. Cahn, Acta Metall. **20**, 423 (1972).
[2] J. Kanamori, Prog. Theor. Phys. **35**, 16 (1966).
[3] M. J. Richards and J. W. Cahn, Acta Metall. **19**, 263 (1971).
[4] F. Ducastelle, in *Cohesion and Structure, Order and Phase Stability in Alloys,* edited by F. R. de Boer and D. G. Pettifor (North-Holland, Amsterdam, 1991), Vol. 3.
[5] R. Kikuchi, Phys. Rev. **81**, 988 (1951).
[6] W. Shockley, J. Chem. Phys. **6**, 130 (1938).
[7] R. H. Fowler and E. A. Guggenheim, *Statistical Thermodynamics* (Cambridge University Press, Cambridge, England,

1960).
[8]K. Binder, *Applications of the Monte-Carlo Methods in Statistical Physics* (Springer-Verlag, Berlin, 1984).
[9]G. D. Mahan and F. H. Claro, Phys. Rev. B **16**, 1168 (1977).
[10]C. Domb, Adv. Phys. **9**, 49 (1960).
[11]J. M. Sanchez, F. Ducastelle, and D. Gratias, Physica **128A**, 334 (1984).
[12]T. Kudō and S. Katsura, Prog. Theor. Phys. **56**, 435 (1976).
[13]A. K. Singh and S. Lele, Philos. Mag. B **65**, 967 (1992).
[14]A. K. Singh and S. Lele, Philos. Mag. B **64**, 275 (1991).
[15]A. K. Singh, V. Singh, and S. Lele, Acta Metall. Mater. **39**, 2847 (1991).
[16]J. Kanamori, J. Phys. Soc. Jpn. **53**, 250 (1984).
[17]J. M. Sanchez and D. de Fontaine, in *Structure and Bonding in Crystals,* edited by M. O'Keefe and A. Navrotsky (Academic, New York, 1981), Vol. 2, p. 117.
[18]J. W. Cahn and R. Kikuchi, Acta Metall. **27**, 1329 (1979).
[19]C. Wolverton, G. Ceder, D. de Fontaine, and H. Dreyssé, Phys. Rev. B **45**, 13 105 (1992).
[20]R. Kikuchi and J. W. Cahn, in *User Applications of Alloy Phase Diagrams,* edited by L. Kaufmann (ASM International, Newbury, OH, 1987).
[21]R. Kikuchi (unpublished).
[22]D. M. Burley, Proc. Phys. Soc. London **85**, 1163 (1965).
[23]G. Ceder, Comput. Mater. Sci. **1**, 144 (1993).
[24]T. Morita, J. Phys. Soc. Jpn. **12**, 753 (1957); J. Math. Phys. **13**, 115 (1972).
[25]J. A. Barker, Proc. R. Soc. London A **216**, 45 (1953).
[26]D. Gratias, J. M. Sanchez, and D. de Fontaine, Physica **113A**, 315 (1982).
[27]G. Ceder, Ph.D. thesis, U.C. Berkeley, 1991 (No. 9203517) available from University Microfilms International, 300 N. Zeeb Rd., Ann Arbor, MI 48106.
[28]M. Asta, C. Wolverton, D. de Fontaine, and H. Dreyssé, Phys. Rev. B **44**, 4907 (1991).
[29]C. Wolverton, M. Asta, H. Dreyssé, and D. de Fontaine, Phys. Rev. B **44**, 4914 (1991).
[30]J. M. Sanchez and D. de Fontaine, Phys. Rev. B **17**, 2926 (1978).
[31]H. Dreyssé, A. Berera, L. T. Wille, and D. de Fontaine, Phys. Rev. B **39**, 2442 (1989).
[32]F. Ducastelle and F. Gautier, J. Phys. F **6**, 2039 (1976).
[33]A. Gonis, X. G. Zhang, A. J. Freeman, P. Turchi, G. M. Stocks, and D. M. Nicholson, Phys. Rev. B **36**, 4630 (1987).
[34]J. W. D. Connolly and A. R. Williams, Phys. Rev. B **27**, 5168 (1983).
[35]T. H. Mattheiss and D. S. Rubin, Math. Oper. Res. **5**, 167 (1980).
[36]M. E. Dyer, Math. Oper. Res. **8**, 381 (1983).
[37]D. Avis and K. Fukuda, in *Proceedings of the 7th ACM Symposium on Computational Geometry* (North Conway, New Hampshire, 1991) (ACM Press, New York, 1991), p. 98.
[38]T. H. Mattheiss, Oper. Res. **121**, 247 (1973).
[39]*Atlas of Crystal Structure Types for Intermetallic Phases,* edited by J. L. C. Daams, P. Villars, and J. H. N. Van Vucht (ASM International, Newbury, OH, 1991).
[40]*Pearson's Handbook of Crystallographic Data for Intermetallic Phases,* 2nd ed., edited by P. Villars and L. D. Calvert (ASTM International, Newbury, OH, 1991).
[41]C. Bichara, S. Crusius, and G. Inden, Physica B **182**, 42 (1992).
[42]C. Wolverton, G. Ceder, D. de Fontaine, and H. Dreyssé, Phys. Rev. B **48**, 726 (1993).
[43]M. Asta, D. de Fontaine, M. Van Schilfgaarde, M. Sluiter, and M. Methfessel, Phys. Rev. B **46**, 5055 (1992).
[44]A. Narita and S. Katsura, Prog. Theor. Phys. **52**, 1448 (1974).
[45]J. Kanamori and Y. Kakehashi, J. Phys. (Paris) Colloq. **38**, C7-274 (1977).
[46]S. Crusius and G. Inden, in *Proceedings of the International Symposium on Dynamics of Ordering in Condensed Matter,* edited by S. Komura and H. Furukawa (Plenum, New York, 1988), p. 139.
[47]C. M. Van Baal, Physica **64**, 571 (1973).
[48]C. Bichara, S. Crusius, and G. Inden, Physica B **179**, 221 (1992).
[49]B. D. Metcalf, Phys. Lett. **45A**, 1 (1973).
[50]R. M. F. Houtappel, Physica **16**, 425 (1950).
[51]G. H. Wannier, Phys. Rev. **79**, 357 (1950).
[52]J. M. Sanchez, D. de Fontaine, and W. Teitler, Phys. Rev. B **26**, 1465 (1982).
[53]A. Finel, in *Alloy Phase Stability,* edited by G. M. Stocks and A. Gonis (Kluwer Academic, Dordrecht, 1989), pp. 269–279.
[54]D. Chandler, *Introduction to Modern Statistical Mechanics* (Oxford University Press, New York, 1987), p. 87.
[55]J. M. Sanchez and D. de Fontaine, Phys. Rev. B **25**, 1759 (1982).
[56]P. Cenedese and J. W. Cahn (private communication).